Applied Catalysis A: General 375 (2010) 295–302

Contents lists available at ScienceDirect

Applied Catalysis A: General

journal homepage: www.elsevier.com/locate/apcata

Nanoscale manganese oxide octahedral molecular sieves (OMS-2) as efficient photocatalysts in 2-propanol oxidation

Aparna Iyer [a], Hugo Galindo [a], Shanthakumar Sithambaram [a], Cecil King'ondu [a], Chun-Hu Chen [a], Steven L. Suib [a,b,*]

[a] Department of Chemistry, University of Connecticut, U-3060, 55 North Eagleville Rd., Storrs, CT 06269-3060, USA
[b] Department of Chemical, Materials, and Biomolecular Engineering, University of Connecticut, U-3060, 55 North Eagleville Rd., Storrs, CT 06269-3060, USA

ARTICLE INFO

Article history:
Received 24 August 2009
Received in revised form 24 December 2009
Accepted 10 January 2010
Available online 15 January 2010

Keywords:
Photocatalysis
Oxidation
Manganese oxide octahedral molecular sieves
Oxygen evolution

ABSTRACT

Crystalline tunnel structure cryptomelane type manganese oxides (OMS-2) have been studied as photocatalysts for the selective oxidation of 2-propanol to acetone. The reaction is carried out with visible light irradiation at room temperature. The activities of various K-OMS-2 and metal doped OMS-2 (M-OMS-2) catalysts prepared by different synthesis procedures have been evaluated. K-OMS-2 and M-OMS-2 (M = Fe, Ni) with nanorod morphology were the most active photocatalysts. Conversions obtained for these catalysts ranged from 50 to 15%. K-OMS-2 fibers gave only 5–6% conversion. All reactions gave 100% selectivity to acetone. The reusability of the K-OMS-2 catalyst was also tested. Characterization of K-OMS-2 catalysts was done using several techniques like temperature programmed desorption, UV–vis spectroscopy, average oxidation state analysis, XRD, BET and FE-SEM. As suggested by the photochemical and characterization data, synthesis methodology, morphology, mixed valency and the release of oxygen from the OMS-2 structure are important factors for the design of active OMS-2 photocatalysts. XRD and FTIR were also used to study structural changes in the catalyst after photolysis.

1. Introduction

Today's increasing energy consumption and depleting fossil fuel resources have compelled us to seek alternative sources of energy. In line with this, harnessing solar energy is unquestionably a viable alternative to conventional technologies using fossil fuels, since solar energy is an abundant natural resource [1,2]. Photocatalytic reactions using solar energy can successfully catalyze mild oxidation of alkanes, alkenes, and alcohols on the surfaces of metal oxides or sulfides. A very important application of such reactions is the destruction of volatile organic compounds in air and water purification processes [3]. Photocatalytic oxidation reactions have several advantages such as use of solar energy as the activation source, stable semiconductor catalysts, room temperature reactions, and the use of non-toxic oxidants like molecular oxygen and air [4,5]. Heterogeneous gas phase catalysis is a particularly simple and environmentally friendly technique due to the ease of recovery of the catalyst and reusability [6]. However, the development of cheap catalysts that can efficiently harness solar energy still remains a huge challenge for chemists [2,7].

Among metal oxides, TiO_2 and ZnO based photocatalysts have been very popular. However, in many cases doping with certain elements is necessary to make them utilizable under visible light irradiation [8,9]. Other transition metal oxides like manganese oxide based photocatalytic systems [10–14] have been studied to a lesser extent even though in nature manganese containing clusters bring about the photo oxidation of water in the presence of sunlight [15]. In manganese oxide, d–d electronic transitions are known to occur during irradiation due to partially filled d-orbitals. So manganese oxide can be effectively used as photocatalyst without the need of doping. The problem of charge confinement in the d-orbital can be overcome by designing nanostructures that will facilitate the easy migration of charge carriers in the oxide [10]. Hence, there lies an opportunity for the development of efficient photocatalysts based on manganese oxide.

K-OMS-2 or manganese octahedral molecular sieves (Fig. 1) are a type of manganese oxide having a highly porous structure and are particularly well known for catalyzing selective oxidation reactions. K-OMS-2 (mineral name – cryptomelane) is constructed from MnO_6 octahedral blocks that form edge-shared double chains and are corner connected to form a tunnel of ~4.7 A by 4.7 A size. The tunnel has a chemical composition of $KMn_8O_{16}{\cdot}nH_2O$ with the K^+ cation residing in the center of the tunnel. The material exhibits salient features like mixed-valency (2+, 3+, and 4+) of Mn, a hydrophobic nature, porous structure, easy release of lattice oxygen, and acidic sites [16]. Several different morphologies have

* Corresponding author at: Department of Chemistry, University of Connecticut, U-3060, 55 North Eagleville Rd., Storrs, CT 06269-3060, USA. Tel.: +1 860 486 2797; fax: +1 860 486 2981.
E-mail address: Steven.Suib@uconn.edu (S.L. Suib).

0926-860X/$ – see front matter © 2010 Elsevier B.V. All rights reserved.
doi:10.1016/j.apcata.2010.01.012

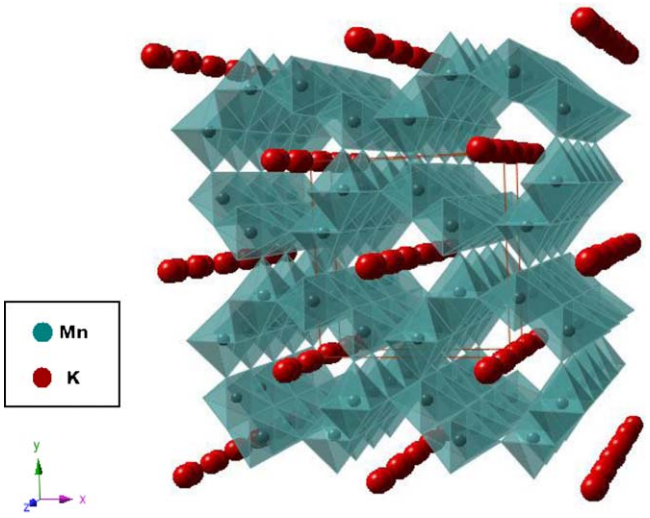

Fig. 1. Tunnel structure of K-OMS-2 or cryptomelane. Each Mn atom (shown in green) is surrounded by 6 O atoms represented by a octahedron. The K atoms (shown in red) occupy the tunnel. (This image was generated using CrystalMaker®: CrystalMaker Software Ltd, Oxford, England (www.crystalmaker.com).) (For interpretation of the references to color in this figure legend, the reader is referred to the web version of the article.)

been synthesized ranging from micrometer long fibers to nanorods and paper like materials [17,18]. These properties make K-OMS-2 an ideal catalyst particularly for a variety of oxidation reactions. Interesting catalytic oxidation reactions have been reported using K-OMS-2 as a catalyst [19–24]. These materials have proven to be highly selective towards organic compounds [25]. Various synthesis procedures, detailed characterization and catalytic studies have been established in our laboratory [16].

Despite the fact that K-OMS-2 is an excellent catalyst for several oxidation reactions, most reactions have been carried out under conditions like conventional heating or microwave irradiation along with harmful peroxides as oxidants [20,22,23]. K-OMS-2 fibers were very poor photocatalysts when irradiated with visible light in the gas phase oxidation of 2-propanol [13]. Under the same conditions, another type of manganese oxide amorphous manganese oxide (AMO) showed higher conversions (~8%) of 2-propanol due to the easy evolution of oxygen from its structure. However, AMO underwent structural changes after photolysis [13]. In this study, the photocatalytic activities of K-OMS-2 and metal doped OMS-2 (M-OMS-2) with different morphologies are examined under visible light irradiation (400–760 nm range), which is similar to the spectral range of the sun. Also, molecular oxygen was used as an oxidant. We have used the gas phase oxidation of 2-propanol as a probe reaction [26–30]. After reaction the catalyst was regenerated by a very simple procedure and reused. Comparative experiments were carried out with K-OMS-2 prepared by other synthesis procedures to evaluate the effect of different morphologies on photocatalytic activity. Temperature programmed desorption techniques were used to study oxygen evolution from K-OMS-2 materials. Characterization of K-OMS-2 catalyst is done before and after reaction to detect any changes in structure after photolysis.

2. Experimental

2.1. Synthesis of K-OMS-2 materials

A solvent free method was used to prepare K-OMS-2_{SF} [17]. The synthesis involved the physical mixing of Mn^{2+} with $KMnO_4$ in the ratio of 2:3. Typically, 90 mmol of $Mn(Ac)_2{\cdot}4H_2O$ and 60 mmol of $KMnO_4$ were ground homogenously in an agate mortar. The mixture was maintained at 120 °C for 4 h in a capped glass bottle. The resulting powders were thoroughly washed with deionized water several times until the pH is close to 7 and dried at 80 °C overnight. Metal doped solvent free (M-OMS-2_{SF}, M = Fe, Ni) catalysts were prepared by mixing $KMnO_4$:$Mn(Ac)_2{\cdot}4H_2O$:metal(II) acetate in a molar ratio of 2:3:0.5. The same procedure described above was followed.

A reflux method [31] was employed to synthesize K-OMS-2_R. In a typical reaction, 37 mmol of $KMnO_4$ was placed in 100 mL of double deionized water (DDW) and added to a solution of 55 mmol of manganese sulfate hydrate in 30 mL DDW. Three milliliter of nitric acid was added to this solution. A dark brown slurry forms which is refluxed for 24 h at a temperature of 110 °C, then filtered, washed and dried at 120 °C overnight.

For the preparation of K-OMS-2_{HY}, a hydrothermal synthesis was used [32]. $K_2S_2O_8$ (1.629 g), K_2SO_4 (1.046 g) and $MnSO_4$ (0.678 g) were added to a Teflon liner with 13 mL DDW. The mole ratio of chemicals is 2:3:3. This solution was stirred for 30 min and put in an autoclave for 48 h at 200 °C. The powder was then washed thoroughly with water and ethanol and dried at 100 °C overnight.

2.2. Catalyst characterization

2.2.1. X-Ray diffraction

X-ray diffraction data were obtained using a Scintag-2000 PDS diffractometer with Cu Kα (λ = 0.15406) radiation. The beam voltage and beam current were set at 45 kV and 40 mA. Continuous scans were taken in a 2θ range of 5–85° with a scan rate of 0.02 °/s. The Joint Committee on Powder Diffraction Society (JCPDS) database was used to index the peaks of XRD. The XRD patterns of K-OMS-2 catalysts are comparable to standard K-OMS-2 materials.

2.2.2. Morphology

The morphologies of the K-OMS-2 materials were studied using a field emission scanning electron microscope (FE-SEM) on a Zeiss DSM 982 Gemini instrument with a Schottky emitter at an accelerating voltage of 2 kV and a beam current of 1 mA. The samples were suspended in ethanol and dispersed on Au–Pd-coated silicon. Transmission electron microscopy (TEM) images were obtained in a Philips EM420 operating at 120 kV. The samples were prepared by dispersing in ethanol and sonicated for 5 min. The suspension was then dropped on a carbon coated copper grid.

2.2.3. Surface area and porosity analysis

The BET surface area analysis and porosity were determined using a Micromeritics ASAP 2010 instrument. All samples were degassed at 120 °C for 10 h to remove any physically adsorbed species. Nitrogen isothermal adsorption and desorption experiments were conducted at relative partial pressures (P/P_0) from 10^{-3} to 0.01, respectively.

2.2.4. Temperature programmed desorption (TPD)

Temperature programmed desorption with mass spectrometric analysis was done to study oxygen evolution from the catalysts before and after catalytic reaction. The catalyst (50 mg) was packed into a tubular furnace controlled by an Omega temperature controller. The sample was purged with UHP argon (Airgas) for 6–8 h at room temperature followed by the heating of the sample to 700 °C at the rate of 10 °C/min. The exhaust gas was fed to a MKS quadrupole mass spectrometer and the evolution of oxygen was monitored.

2.2.5. FTIR

Fourier transform infrared (FTIR) spectroscopy experiments were performed on a Nicolet 750 spectrometer with a Mercury–

Cadmium–Telluride (MCT) detector and KBr beam splitter. Spectra were collected with a resolution of 4 cm^{-1} using 250 scans.

2.2.6. Average oxidation state

Potentiometric titration was used to measure the average oxidation state (AOS) of the K-OMS-2 catalysts. The catalyst was dissolved in hydrochloric acid so as to convert all the manganese to Mn^{2+} and titrated to a Mn^{3+} complex with sodium pyrophosphate versus potassium permanganate. This gives total Mn content, based on which the AOS is determined by reducing the solid to Mn^{2+} using ferrous ammonium sulfate and back-titrating the excess Fe^{2+} with a permanganate standard.

2.3. Photocatalytic reactions

The photocatalytic activity of the K-OMS-2 materials was tested in the presence of visible light under heterogeneous conditions. Prior to every reaction the catalyst surface was cleaned in a continuous stream of argon for 2 h. Oxidation of 2-propanol was carried out using 50 mg of catalyst in a quartz tube with 13 mm diameter. A 1000 W continuous output xenon lamp was used to illuminate the catalyst bed. Lamp power was controlled at 520 W. The UV radiation coming from the source was cut-off by a 400-nm filter and the IR was cut-off using a glass water filter to keep the reaction system from heating. 2-Propanol was bubbled from an ice-bath constantly maintained at 0 °C. Molecular oxygen flown at the rate of 10 mL/min was used as a carrier gas. An online gas chromatograph connected to the reactor was used to analyze the reaction products. GC analyses were done using a HP 5890 series II gas chromatograph with a flame ionization detector. A HP Plot Q column (bonded polystyrene-divinylbenzene column) of dimensions 30 m × 0.53 mm I.D. × 40 μm film was used.

3. Results

3.1. Characterization of OMS-2 catalysts

3.1.1. Characterization of undoped K-OMS-2 catalysts

SEM images for K-OMS-2 materials synthesized in this study are shown in Fig. 2. K-OMS-2_{SF} (Fig. 2a) prepared by solvent free method has nanorod morphology with a particle width of about 10 nm. The lengths of these rods vary from 30 to 100 nm. K-OMS-2_R (Fig. 2b) has fiber morphology and the length of these fibers is greater than 1000 nm. Based on SEM images, these fibers have

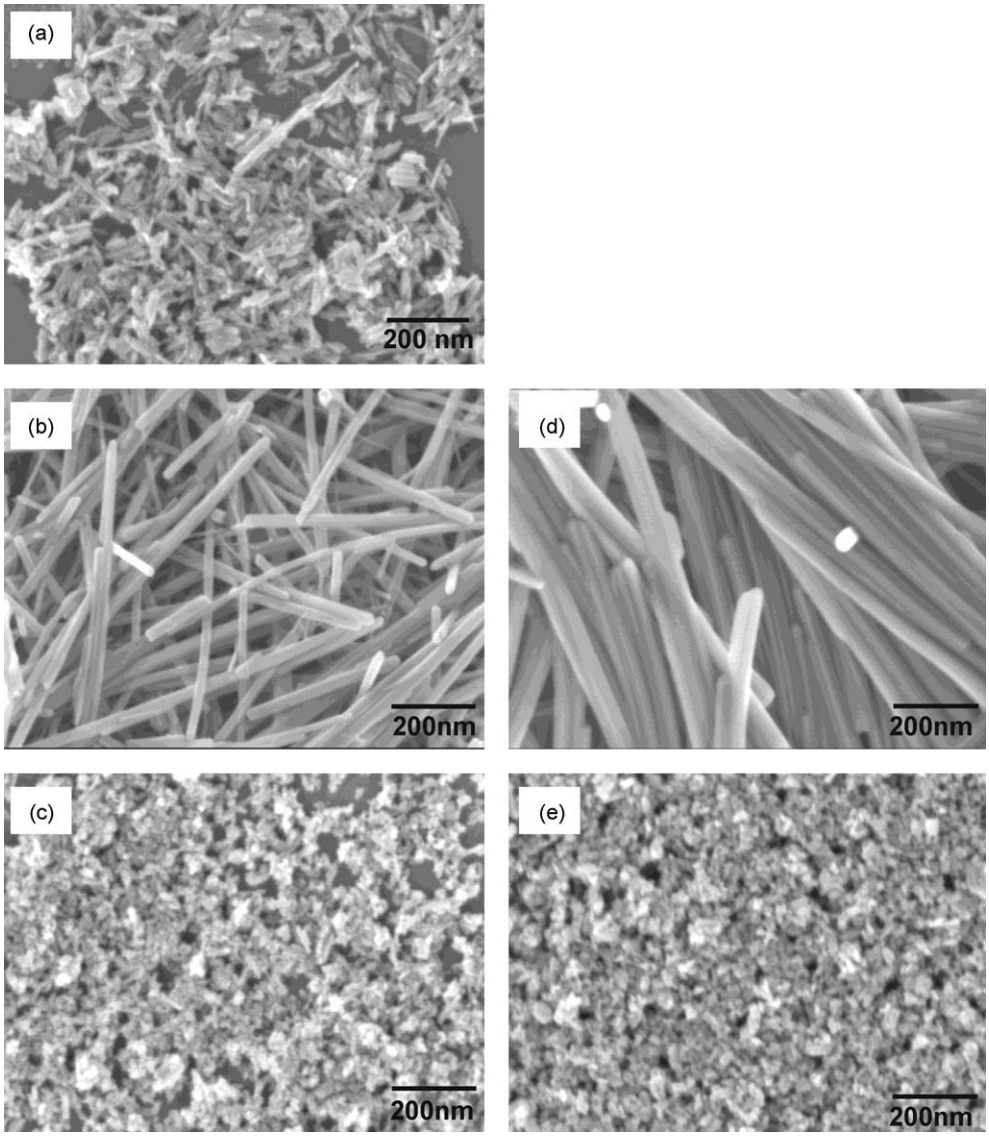

Fig. 2. SEM images of as-synthesized OMS-2 catalysts: (a) K-OMS-2_{SF}, (b) K-OMS-2_R, (c) K-OMS-2_{HY}, (d) Fe-OMS-2_{SF} and (e) Ni-OMS-2_{SF}.

width of approximately 15–30 nm. The hydrothermal synthesis (Fig. 2c) yielded fibers with widths of few tens of nanometers (approx. 15–30 nm) and lengths of several micrometers. TEM images (S1) representing individual nanorods and individual fibers are given from which the approximate width of the fibers and rods can be confirmed.

The X-ray diffraction patterns of K-OMS-2 catalysts prepared by various synthesis procedures (reflux, hydrothermal, solvent free) are in good agreement with the standard pattern of pure cryptomelane (Fig. 3). All peaks can be indexed to pure cryptomelane phase (JCPDS 29-1020) and no other phases are present. The peaks for K-OMS-2_{SF} are much broader and weaker than those for K-OMS-2_R and K-OMS-2_{HY} indicating smaller crystallite size. K-OMS-2_{SF} has the smallest crystallite size (9.8 nm) [17] as shown in Table 1. This value from earlier work on OMS-2, had been calculated using the Scherrer equation for the (2 1 1) peak from XRD data [17,20]. The BET surface areas, porosity values and crystallite sizes of all catalysts are tabulated in Table 1. Among all K-OMS-2 catalysts, K-OMS-2_{SF} has the highest surface area (123 m^2/g), highest mesopore volume (94%), and the smallest crystallite size.

3.1.2. Characterization of doped OMS-2 catalysts prepared by solvent free method

SEM images of doped catalysts (Fe-OMS-2_{SF} (Fig. 2d) and Ni-OMS-2_{SF} (Fig. 2e)) are shown. The images show nanorod morphology as for the undoped K-OMS-2_{SF}. In addition, no other phases are seen in the image.

The XRD patterns (Fig. 3) of the doped catalysts (Fe-OMS-2_{SF} and Ni-OMS-2_{SF}) match well with cryptomelane and no additional phases are present for the doped materials. Crystallite size calculation was done using the Scherrer equation and the (2 1 1) XRD peak. Fe-OMS-2_{SF} has a crystallite size of 10.8 nm and Ni-OMS-2_{SF} has a size of 12 nm (Table 1). These values are close to the crystallite size of K-OMS-2_{SF} [17] (Table 1). The surface areas and porosity values presented in Table 1 show that the doped catalysts have high surface area (168 m^2/g and 109 m^2/g for Fe-OMS-2_{SF} and Ni-OMS-2_{SF}, respectively) and high mesopore volume (Table 1) in the structure.

3.2. Photocatalytic reactions with various OMS-2 materials

Results for the photocatalytic oxidation of 2-propanol using different K-OMS-2 catalysts prepared by reflux, solvent free and hydrothermal methods are shown in Fig. 4. In all cases, the reaction is selective and only acetone was detected as the partial oxidation product. Among all the catalysts tested, K-OMS-2_{SF} gave the highest conversion. Fig. 4 shows that the activity of K-OMS-2_{SF} is very high ~50% at the beginning of the reaction, then decreases to 15% conversion to acetone as time proceeds. However, the catalytic activity was maintained for more than 4 h. In order to check for total oxidation of 2-propanol as a possibility, the same reaction was carried out and analysis was conducted using a SRI GC equipped with a TCD detector. CO_2 was not detected as a product of the reaction. Hence the reaction with K-OMS-2 materials is 100% selective. Other catalysts, i.e. K-OMS-2_R and K-OMS-2_{HY} showed poor photocatalytic activity (only 5–6%) when tested under the same conditions (Fig. 4).

Since K-OMS-2_{SF} showed the highest photocatalytic activity, metal doped OMS-2 (Fe-OMS-2_{SF} and Ni-OMS-2_{SF}) catalysts

Table 1
Properties of as-synthesized K-OMS-2 catalysts.

Catalyst	Crystallite size (nm)	Surface area (m^2/g)	Mesopore vol. (cm^3/g)	Total pore vol. (cm^3/g)	% mesopore vol.
K-OMS-2_{SF}	9.8[a]	123	0.33	0.35	94%
K-OMS-2_R[a]	18	90	0.29	0.46	63%
K-OMS-2_{HY}	17[b]	57	0.19	0.22	86%
Fe-OMS-2_{SF}	10.8	168	0.54	0.56	96%
Ni-OMS-2_{SF}	12	109	0.30	0.33	90%

[a] Ref. [17].
[b] Ref. [20].

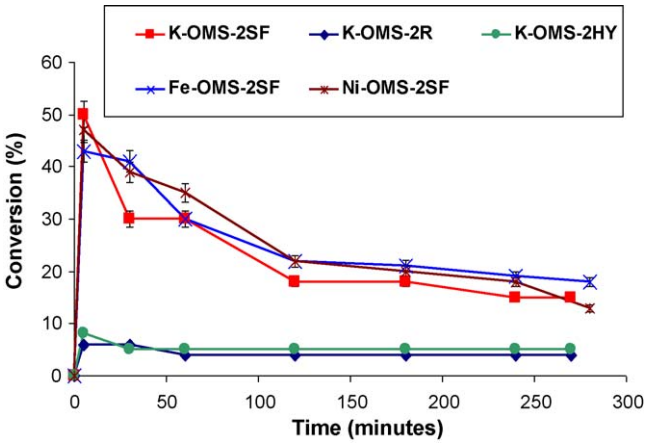

Fig. 4. Conversion of 2-propanol to acetone using K-OMS-2 and metal doped OMS-2_{SF} catalysts under visible light. Reaction conditions: 50 mg of catalyst, 2-propanol at 0 °C, O_2 flow rate = 10 mL/min, lamp power = 520 W.

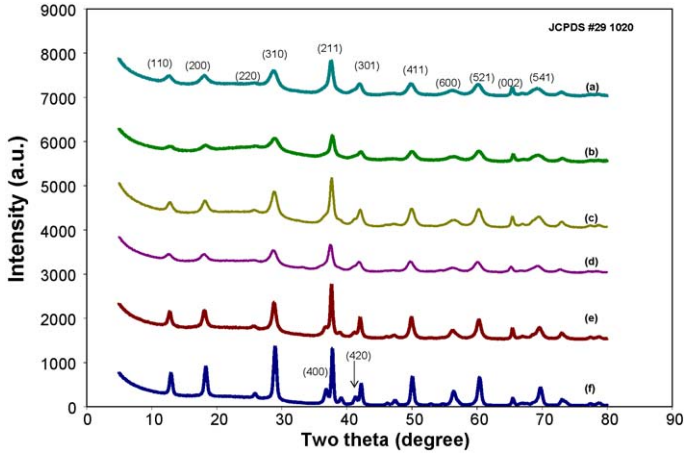

Fig. 3. X-Ray diffraction patterns: (a) fresh K-OMS-2_{SF}, (b) K-OMS-2_{SF} after photoreaction, (c) fresh Ni-OMS-2_{SF}, (d) fresh Fe-OMS-2_{SF}, (e) fresh K-OMS-2_R and (f) fresh K-OMS-2_{HY}.

Table 2
Reusability test for photocatalytic oxidation of 2-propanol.

Time (min)	Conversion of 2-propanol (%)		
	Fresh K-OMS-2_{SF}	Used K-OMS-2_{SF} recycled after heating at 240 °C	Used K-OMS-2_{SF} recycled after heating at 120 °C
15	50	37	8
30	30	24	2
60	30	26	2
90	18	15	2
120	18	14	1
240	15	14	3

Reaction conditions: 50 mg of catalyst, 2-propanol at 0 °C, O_2 flow rate = 10 mL/min, lamp power = 520 W.

prepared by solvent free method were also tested for photocatalytic conversion of 2-propanol. The results are displayed in Fig. 4. Doped materials prepared by solvent free method showed ~50–20% conversions to acetone which is similar to the undoped catalyst.

3.3. Catalyst reusability

Since K-OMS-2_{SF} showed the highest photocatalytic activity, the reusability of the K-OMS-2_{SF} was tested. This is shown in Table 2. After completing the reaction with fresh K-OMS-2_{SF}, the catalyst was heated at 240 °C or 120 °C overnight to remove any adsorbed species. The catalytic activity recovered almost completely after treatment at 240 °C. However, when the reusability test was conducted by heating the used catalyst at 120 °C overnight and tested for the same reaction, the catalyst showed a significant decrease in activity.

3.4. Temperature programmed desorption (TPD-MS)

In order to study oxygen evolution from the catalyst surface, the K-OMS-2 materials were heated in an inert (argon) atmosphere and the oxygen evolving from the surface was monitored using mass spectrometry. TPD-MS profiles are displayed in Fig. 5. Among the three catalysts tested, K-OMS-2_{SF} shows predominant evolution of oxygen starting above 500 °C. Even though quantification of oxygen evolved was not done, Fig. 5 shows that the intensity of the oxygen peak evolved from the surface of K-OMS-2_{SF} catalyst is much higher than those for K-OMS-2_R and K-OMS-2_{HY}. In the case of K-OMS-2_R, a small shoulder is seen above 400 °C and an oxygen peak evolves around 540 °C. In K-OMS-2_{HY}, oxygen begins to evolve around 500 °C beginning with a small shoulder. The K-OMS-2_{SF} oxygen peak is markedly different from those of K-OMS-2_{HY} and K-OMS-2_R in that a lower temperature peak (below 400 °C) was not seen. An O_2 peak rises sharply just above 500 °C. This peak is followed by another hump which evolved at a higher temperature than 700 °C but this is not displayed in the figure.

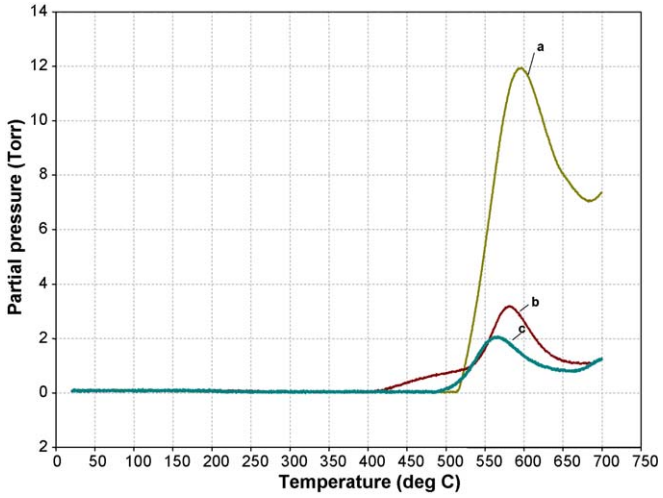

Fig. 5. TPD-MS profiles of m/e = 32 for various K-OMS-2 catalysts: (a) K-OMS-2_{SF}, (b) K-OMS-2_R and (c) K-OMS-2_{HY}.

4. Discussion

4.1. Structural considerations

Nanoscale manganese oxides absorb photons in the 400-nm region [11]. The band gap energy is the energy between the Mn 3d t_{2g} and e_g states [10]. K-OMS-2 is an indirect semiconductor oxide. Bulk MnO_2 has a band gap of 0.2 eV. K-OMS-2 nanofibers have a band gap of 1.32 eV which is ~1 eV blue shifted with respect to bulk materials [33]. The estimated band gap of MnO_2 monolayer nanosheets is 2.23 eV [10]. Hence, the electronic structure and the size of fibers greatly affect the band gap energy and this in turn affects photocatalytic activity [33].

A study done with TiO_2 catalysts reported that the photocatalytic activity increased with particle size up to ~30 nm and beyond that the activity decreased as the particle size increased for TiO_2 catalysts [34]. Such an effect may exist in K-OMS-2_R and K-OMS-2_{HY} where the very long hollow fiber morphology allowed electron–hole recombination to occur more easily inside the particle and hence prevented the efficient diffusion of charge carriers to the surface. Sakai et al. [10] have noted that ultrathin nanosheets provide a better surface for d–d transitions due to facilitation the easy migration of holes and electrons to the surface of the oxide [10]. The unique nanorod morphology and small crystallite size of ~9.8 nm of K-OMS-2_{SF} readily allows easy electron transfer in the catalyst when irradiated. Efficient hydrolysis of nitriles was catalyzed under light with α-MnO_2 nanorods of ~75 nm diameter and ~235 nm length [11]. Due to the unique structure of OMS-2_{SF} nanorods, they are the most active catalysts for oxidation of various alcohols among all K-OMS-2 materials [17,22]. The catalytic activity did not show any particular trend with surface area. K-OMS-2_R (90 m^2/g) and K-OMS-2_{HY} (57 m^2/g) have very similar catalytic activity even though their surface areas vary greatly.

Incorporation of dopant ions (Fe and Ni) into OMS-2_{SF} did not significantly change but improved the conversion to acetone slightly compared to undoped catalyst made by the solvent free method as seen in Fig. 4. In metal doped OMS-2 catalysts, the catalytic activity could vary compared to the undoped ones depending on different oxidation states, accessibility of the transition metals and defects in the OMS-2 structure due to the foreign cations [35,36]. However, in this case, the amount of dopants present in the catalyst could be too low to bring about any significant change. An optimization study is further required to understand the effect of amount of dopant.

4.2. Mixed valency in manganese oxides

OMS-2 has bands in the visible region (488 nm and 542 nm) that are d–d transitions in Mn^{4+} ($^2t_{2g}$ to ^3e_g) and Mn^{3+} (^5E to $^5T_2$), respectively [12]. The presence of both these species could be important for enhanced photocatalytic activity due to light induced semi-conductivity in Mn^{3+}:Mn^{4+} [37]. The electrical conductivity of K-OMS-2_{SF} measured using a 4 probe d.c. Van der Pawv technique was found to be $8.3 \times 10^{-3}\ \Omega^{-1}\ cm^{-1}$. The average oxidation state of various K-OMS-2 catalysts was also

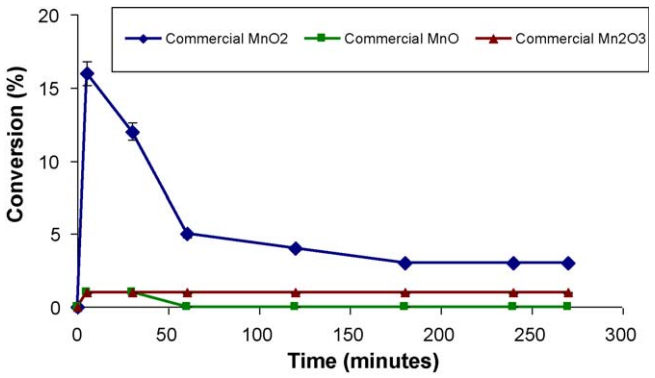

Fig. 6. Photocatalytic activity of commercial manganese oxides: (a) commercial MnO_2, (b) commercial Mn_2O_3 and (c) commercial MnO. Reaction conditions: 50 mg of catalyst, 2-propanol at 0 °C, O_2 flow rate = 10 mL/min, lamp power = 520 W.

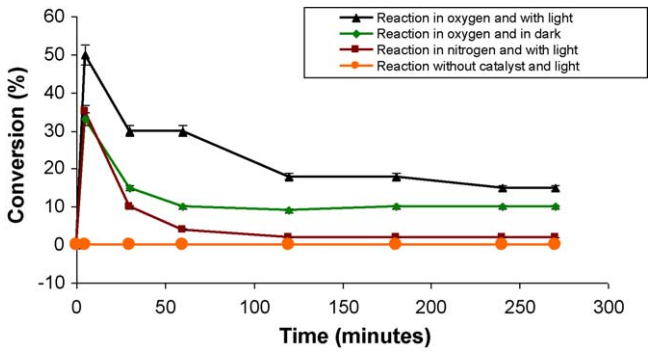

Fig. 7. Effect of light and oxygen on the activity of K-OMS-2_{SF} catalyst. Reaction conditions: 50 mg of catalyst, 2-propanol at 0 °C, O_2 flow rate = 10 mL/min, lamp power = 520 W.

measured. The AOS values varied over a small range, i.e. 3.79–3.91. K-OMS-2_{SF} has the smallest AOS number of 3.79 compared to the AOS numbers for other two catalysts viz. K-OMS-2_R (AOS = 3.91) and K-OMS-2_{HY} (AOS = 3.91). This could indicate that even a slight proportional difference of Mn^{3+} to Mn^{4+} could enhance photocatalytic activity since Mn^{3+} and Mn^{4+} have different electronic structure and hence would have different effects on the band gap of K-OMS-2 nanomaterials [33]. Tests were also conducted with commercial manganese oxides – MnO_2, Mn_2O_3 and MnO. Commercial MnO_2 was the most active among the three catalysts (Fig. 6). The activity of commercial MnO_2 decreased after a few minutes of reaction (conversion to acetone fell from 15 to 4%). Mn_2O_3 showed very poor activity (only 3% conversion) and MnO did not show any conversion.

4.3. Oxygen evolution from K-OMS-2 catalysts

Oxygen evolution from K-OMS-2 catalysts was studied using TPD-MS (Fig. 5). TPD-MS profiles show the peak intensities of oxygen evolved from various catalysts when heated in an argon stream. The oxygen peak patterns agree closely with the spectra of K-OMS-2 catalysts recorded by Makwana et al. [38]. Oxygen peaks from K-OMS-2 materials can be categorized into low temperature (LT) peaks, medium temperature (MT) peaks and high temperature (HT) peaks [39,40]. The LT peaks are due to chemisorbed oxygen on the catalyst surface. The medium temperature peaks are due to oxygen evolving from the lattice layers very close to the catalyst surface [38]. The loss of oxygen at this point does not lead to the complete breakdown of the cryptomelane tunnel structure. A small number of vacancies form on the surface due to oxygen mobility [25]. The peak evolved from fresh K-OMS-2_{SF} just above 500 °C is the MT peak and is the highest amount of lattice oxygen evolved from the catalyst surface compared to other K-OMS-2 catalysts. This property of easy evolution of lattice oxygen from the surface of K-OMS-2_{SF} catalyst could play an important role in its photocatalytic activity. The decomposition of the material starts to occur above 700 °C. Easy evolution of lattice oxygen could also be due to strain in the Mn–O bonds due to the presence of more Mn^{3+} species in the catalyst [38].

There are two different mechanisms suggested for the photo oxidation of 2-propanol. In one mechanism, the photo-adsorbed oxygen [$O_2^{-}{}_{(ads)}$] from gas phase oxygen reacts with $^{\bullet}OH$ radicals on the catalyst surface to form $^{\bullet}OH_2$ radical species that carry out the photo oxidation process [29]. In another mechanism, the lattice oxygen or surface hydroxyl groups form excited oxygen species in the presence of irradiation due to electron transfer in the manganese oxide structure. These species bring about the oxidation reaction of the alcohols [27]. The probable mechanism on K-OMS-2 catalysts could be the second mechanism in which the lattice oxygen or radical hydroxyl species first participate in the reaction. In the case of K-OMS-2_{SF} when reaction was carried out in an inert atmosphere (nitrogen) the catalyst still showed activity even though no gas phase oxygen is supplied (Fig. 7). However, the catalyst deactivated very quickly implying that the oxygen from the manganese oxide and walls of reactor is first consumed for photocatalytic oxidation but later needs to be replenished by molecular oxygen. Reaction carried out with gas phase oxygen and light but without any catalyst showed no conversion of 2-propanol. In the absence of irradiation, the reaction still occurs. However, the conversion at the beginning of the reaction is only 30% and deactivates to 10% which is much lower than in the presence of irradiation (50–15%) (Fig. 7). These results are similar to those reported for the photocatalytic oxidation of 2-propanol using amorphous manganese oxide [13]. Hence, lattice oxygen is important for the oxidation process on the manganese oxide surface.

Three key steps involved in the oxidation process are electron transfer due to light absorption by the manganese oxide, reduction of manganese species and movement of oxygen from the bulk to the surface and re-oxidation of manganese oxide by gas phase oxygen [13]. The proposed mechanism is depicted in Scheme 1. Larson et al. [27] studied the involvement of lattice oxygen on the surface during the photo oxidation of 2-propanol with titanium oxide (Degussa P-25) and reported that when less than a stoichiometric quantity of oxygen is supplied during the reaction, the balance oxygen needed for the reaction was supplied from the TiO_2 catalyst surface indicating that lattice oxygen is involved in the photo oxidation process [27].

The photo degradation pathway of 2-propanol has been proposed to occur through a dehydrogenation pathway to form acetone without the formation of propene [27]. Studies suggest that degradation occurs through the formation of 2-propoxide as an intermediate leading to acetone as the major product [28]. However, this species was not detected in our GC analysis. Acetone further undergoes oxidation to form mesityl oxide and probably acetic acid which ultimately decomposes to CO_2 however this reaction takes place at a relatively slower rate [28]. Our analysis did not show the formation of CO_2 during the reaction. No other products except acetone were detected. With the use of Degussa P-25 as a catalyst, the photocatalytic oxidation products of 2-propanol are known to be acetone, H_2O, and CO_2 [27]. 100% selectivity to acetone was also reported by Cao and Suib [13] using amorphous manganese oxide and no CO_2 formation was detected. Partial oxidation to acetone instead of complete mineralization could be due to the fact that not enough energy is supplied by visible light.

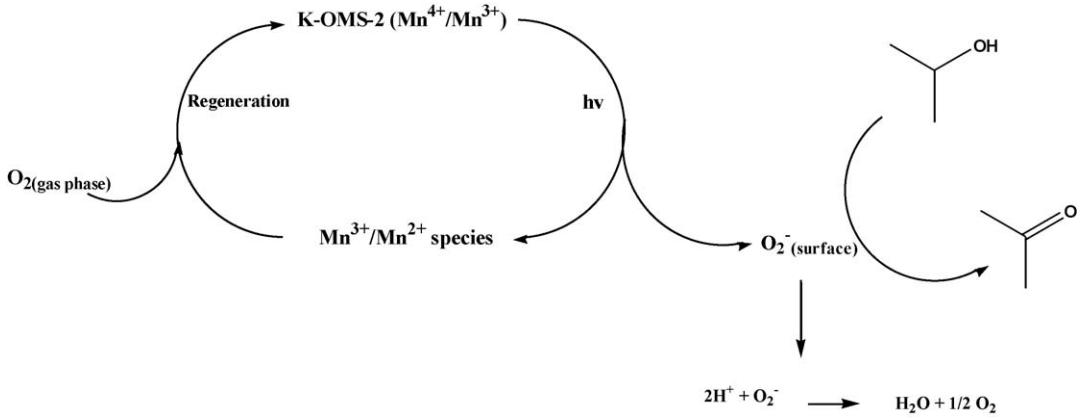

Scheme 1. Proposed cycle of photo oxidation of 2-propanol on the surface of K-OMS-2 catalyst.

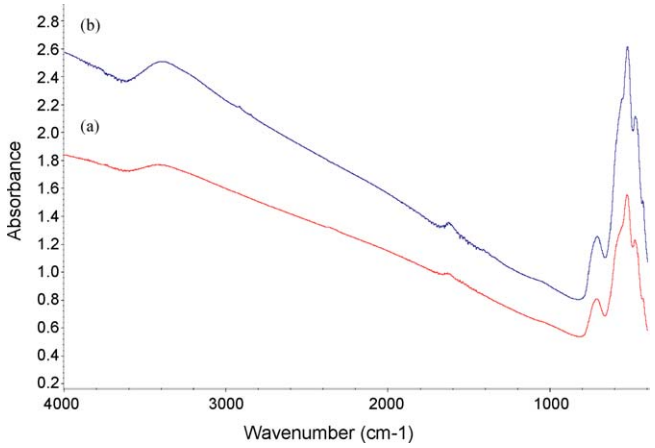

Fig. 8. FTIR spectra of K-OMS-2_{SF} catalyst: (a) before photo reaction and (b) after photo reaction.

4.4. Catalyst deactivation and reusability

Acetone formed on the catalyst surface desorbs very slowly at room temperature and heating is required to completely remove this product [27]. This could be one of the reasons for poisoning of catalytic sites since K-OMS-2 has a very porous structure as suggested by BET data (Table 1) along with occupancy of the tunnel. The deactivated catalyst was tested for reusability and structural changes. Heating the deactivated catalyst at 120 °C overnight did not lead to complete recovery of activity but did show little conversion (<5%) to acetone (Table 2). However, when the catalyst was heated at 240 °C the activity recovered completely showing that organic molecules desorb at this temperature (Table 2). This shows that the catalyst is reusable.

The X-ray diffraction (XRD) patterns of K-OMS-2_{SF} (Fig. 3) catalysts taken before and after the reaction remained unchanged indicating that irradiation did not cause breakdown of the structure of the catalyst. The intensity and peak widths of the used catalyst remained the same as those before reaction.

FTIR spectra were recorded before and after photocatalytic oxidation. The spectra were taken after cleaning the catalyst surface by purging with N_2 overnight. FTIR data are presented in Fig. 8. The spectra taken before and after reactions indicate that there are no structural changes in the catalysts after the reaction. No externally adsorbed species were detected on the catalyst surface.

5. Conclusions

In summary, cryptomelane type manganese oxide (K-OMS-2) with a tunnel structure and unique nanorod morphology, prepared by solvent free technique, is found to be an efficient reusable photocatalyst. K-OMS-2_{SF} (synthesized by solvent free method) successfully catalyzed the gas phase photo oxidation of 2-propanol giving 50–15% conversion to acetone with 100% selectivity under facile reaction conditions like irradiation at ~400 nm to 760 nm and with molecular oxygen as the oxidant. Under the same conditions K-OMS-2 fibers gave only ~5-6% conversion. Enhanced photocatalytic behavior of K-OMS-2_{SF} compared to other K-OMS-2 catalysts may be attributed to its small crystallite size, nanorod morphology, easy evolution of lattice oxygen as shown by TPD data and Mn^{4+}:Mn^{3+} ratio. The catalytic activity recovers completely after being heated at 240 °C overnight. XRD and FTIR characterization of catalysts after photoreaction suggest that the catalyst can withstand irradiation and there was no subsequent change in the structure of the catalyst. Hence, K-OMS-2_{SF} can be successfully used as a reusable photocatalyst. Such OMS-2 photocatalysts with easy inexpensive synthesis procedures, easy recovery, reusability and without the need of physical supports are important and suitable candidates for potential solar energy conversion.

Acknowledgements

We acknowledge support of the Chemical Sciences, Geosciences and Biosciences division, Office of Basic Energy Sciences, Office of Science, U.S. Department of Energy. We would like to thank Dr. Francis Galasso and Dr. Raymond Joesten for helpful discussions. We would also like to thank Linping Xu, Hui Huang and Lei Jin for their support and help.

Appendix A. Supplementary data

Supplementary data associated with this article can be found, in the online version, at doi:10.1016/j.apcata.2010.01.012.

References

[1] M. Kitano, M. Matsuoka, M. Ueshima, M. Anpo, Appl. Catal. A 325 (2007) 1–14.
[2] G.W. Crabtree, N.S. Lewis, Phys. Today 60 (2007) 37–42.
[3] J.M. Herrmann, Top. Catal. 34 (2005) 49–65.
[4] W. Xu, D. Raftery, J. Phys. Chem. B 105 (2001) 4343–4349.
[5] G.B. Raupp, C.T. Junio, Appl. Surf. Sci. 72 (1993) 321–327.
[6] K. Yamaguchi, N. Mizuno, Angew. Chem., Int. Ed. 41 (2002) 4538–4542.
[7] N.S. Lewis, D.G. Nocera, Proc. Natl. Acad. Sci. U.S.A. 103 (2006) 15729–15735.
[8] T. Ohno, Z. Miyamoto, K. Nishijima, H. Kanemitsu, F. Xueyuan, Appl. Catal. A 302 (2006) 62–68.

[9] M. Anpo, Pure Appl. Chem. 72 (2000) 1265–1270.
[10] N. Sakai, Y. Ebina, K. Takada, T. Sasaki, J. Phys. Chem. B 109 (2005) 9651–9655.
[11] S. Jana, S. Praharaj, S. Panigrahi, S. Basu, S. Pande, C. Chang, T. Pal, Org. Lett. 9 (2007) 2191–2193.
[12] M. Alvarez Lemus, T. Lopez, S. Recillas, D.M. Frias, M. Montes, J.J. Delgado, M.A. Centeno, J.A. Odriozola, J. Mol. Catal. A: Chem. 281 (2008) 107–112.
[13] H. Cao, S.L. Suib, J. Am. Chem. Soc. 116 (1994) 5334–5342.
[14] J. Chen, J.C. Lin, V. Purohit, M.B. Cutlip, S.L. Suib, Catal. Today 33 (1997) 205–214.
[15] J.F. Allen, W. Martin, Nature (London, UK) 445 (2007) 610–612.
[16] S.L. Suib, J. Mater. Chem. 18 (2008) 6001.
[17] Y. Ding, X. Shen, S. Sithambaram, S. Gomez, R. Kumar, V.M.B. Crisostomo, S.L. Suib, M. Aindow, Chem. Mater. 17 (2005) 5382–5389.
[18] J. Yuan, K. Laubernds, J. Villegas, S. Gomez, S.L. Suib, Adv. Mater. 16 (2004) 1729–1732.
[19] S.R. Segal, L. Cao, S.L. Suib, X. Tang, S. Satyapal, J. Catal. 198 (2001) 66–76.
[20] R. Ghosh, X. Shen, J.C. Villegas, Y. Ding, K. Malinger, S.L. Suib, J. Phys. Chem. B 110 (2006) 7592–7599.
[21] G.G. Xia, Y.G. Yin, W.S. Willis, J.Y. Wang, S.L. Suib, J. Catal. 185 (1999) 91–105.
[22] S. Sithambaram, E.K. Nyutu, S.L. Suib, Appl. Catal. A 348 (2008) 214–220.
[23] R. Kumar, S. Sithambaram, S.L. Suib, J. Catal. 262 (2009) 304–313.
[24] F. Schurz, J.M. Bauchert, T. Merker, T. Schleid, H. Hasse, R. Glaeser, Appl. Catal. A 355 (2009) 42–49.
[25] J. Luo, Q. Zhang, J. Garcia-Martinez, S.L. Suib, J. Am. Chem. Soc. 130 (2008) 3198–3207.
[26] U.R. Pillai, E. Sahle-Demessie, J. Catal. 211 (2002) 434–444.
[27] S.A. Larson, J.A. Widegren, J.L. Falconer, J. Catal. 157 (1995) 611–625.
[28] W. Xu, D. Raftery, J.S. Francisco, J. Phys. Chem. B 107 (2003) 4537–4544.
[29] R.I. Bickley, R.K.M. Jayanty, Faraday Discuss. Chem. Soc. 58 (1975) 194–204.
[30] G. Marci, E. Garcia-Lopez, L. Palmisano, Catal. Today 144 (2009) 42–47.
[31] R.N. DeGuzman, Y. Shen, E.J. Neth, S.L. Suib, C. O'Young, S. Levine, J.M. Newsam, Chem. Mater. 6 (1994) 815–821.
[32] M. Polverejan, J.C. Villegas, S.L. Suib, J. Am. Chem. Soc. 126 (2004) 7774–7775.
[33] T. Gao, M. Glerup, F. Krumeich, R. Nesper, H. Fjellvag, P. Norby, J. Phys. Chem. C 112 (2008) 13134–13140.
[34] C.B. Almquist, P. Biswas, J. Catal. 212 (2002) 145–156.
[35] T. Sriskandakumar, N. Opembe, C. Chen, A. Morey, C. King'ondu, S.L. Suib, J. Phys. Chem. A 113 (2009) 1523–1530.
[36] X. Chen, Y. Shen, S.L. Suib, C.L. O'Young, J. Catal. 197 (2001) 292–302.
[37] D.M. Sherman, Geochim. Cosmochim. Acta 69 (2005) 3249–3255.
[38] V.D. Makwana, L.J. Garces, J. Liu, J. Cai, Y. Son, S.L. Suib, Catal. Today 85 (2003) 225–233.
[39] Y. Yin, W. Xu, R. DeGuzman, Y. Shen, S.L. Suib, C.L. O'Young, Stud. Surf. Sci. Catal. 84 (1994) 453–460.
[40] Y. Yin, W. Xu, Y. Shen, S.L. Suib, C.L. O'Young, Chem. Mater. 6 (1994) 1803–1808.